

Analog Signal Processing for Large Area SiPM in Cherenkov Telescope Camera

Shobha K. Rao^a, K. S. Gothe^{a,*}, S. S. Upadhy^a, N. K. Parmar^a, R. L. Deshmukh^a, B. B. Singh^a, Sandeep Kumar^a, M. Ranjan^a, A. Sarkar^{a,b}, S. R. Patel^{a,b} and V. R. Chitnis^a

^aTata Institute of Fundamental Research, Homi Bhabha Road, Mumbai, 400005, Maharashtra, India

^bDeutsches Elektronen-Synchrotron, Platanenallee 6, D-15738, Zeuthen Germany

ARTICLE INFO

Keywords:

G-APD, SiPM, preamplifier, IACT, Camera, Front-end

ABSTRACT

We have developed a preamplifier which processes signals from large area pixel sensors each comprising a 4×4 array of SiPMs. These amplifiers constitute a front-end portion of 256 pixel camera for an Imaging Atmospheric Cherenkov Telescope (IACT). The camera would be mounted at the focal plane of the 4-m class telescope. The primary design objective of the camera is to detect wide energy range of the Cherenkov photons guided on to each pixel sensor arriving in a brief flash of a few nanoseconds duration. The other important objective of the camera is to be able to resolve single photon response for accurate pixel gain calibration. There are several factors like long tail portion of the detector signal, large night sky background, high detector capacitance, need to deal with 16 SiPM signals to form a pixel signal, requirement of low components count and power, limited space etc., which have led to a customized design of the preamplifier. We have made use of a judicious combination of the design strategies and circuit ideas to accomplish the design goals. The paper describes the design features of the preamplifier and performance evaluation.

1. Introduction

A prototype 256 pixel camera based on SiPM as photon sensor is being developed for a 4-m class TACTIC (TeV Atmospheric Cherenkov Telescope with Imaging Camera) telescope[1] at Mt Abu, Rajasthan, India. The telescope (Figure 1) is designed to detect the celestial Very High Energy (VHE) gamma rays using imaging atmospheric Cherenkov technique.

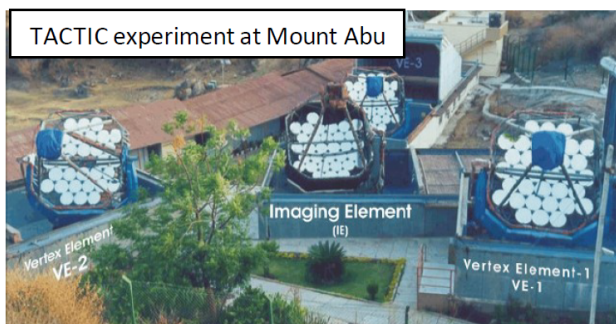


Figure 1: TACTIC array at Mt Abu (Rajasthan, India). The camera under development would be installed in one of the vertex elements of the array. Courtesy: Astrophysical Sciences Division, Bhabha Atomic Research Centre


When the VHE gamma rays or energetic cosmic rays interact with the atmosphere, a cascade of relativistic charged particles is produced. The cascade generates a very short flash of Cherenkov radiation lasting for few nanoseconds. IACT works by capturing the images of these Cherenkov flashes using a pixelated camera placed at the focal plane

of the telescope. The recorded images are then analysed to differentiate between the gamma ray events and cosmic ray events. Eventually, the camera would be deployed on a telescope at Hanle (Ladakh, India) where it would be operating concurrently with MACE telescope[2].

The benefits of SiPM as a pixel sensor was successfully demonstrated first time by FACT which uses 1440 SiPMs as pixel sensors each of size 3 mm × 3 mm [3]. SST-1M of CTA has also reported their camera design that uses large size custom SiPM as a pixel sensor wherein the sensor is divided into 4 channels each of area 23 mm² [4]. The camera described in this paper comprises large size (13 mm × 13 mm), 4×4 array of SiPMs (Hamamatsu S13361-3050AS04) as a "pixel sensor". Each SiPM in the array, referred to as a "subpixel", is of the size 3 mm × 3 mm. The effective sensor area of the camera is 144 mm². The matrix of 256 pixel sensors mounted on the camera front-end is shown in figure 2. The figure also illustrates the pixel sensor and corresponding subpixels.

Table 1 shows relevant specifications of the sensor given by the manufacturer[5]. All the sixteen SiPMs in a pixel sensor are operated by applying a common reverse bias voltage beyond their breakdown voltages. A photon incident on a subpixel may trigger an avalanche generating a current pulse. The charge delivered by the current pulse depends on the overvoltage (applied bias voltage minus breakdown voltage). For a given overvoltage, the total charge delivered by a subpixel is proportional to the number of avalanches and therefore to the number of photons incident on that subpixel. Each channel of the 4 channel preamplifier described in the paper processes current pulses from 16 "subpixels" of a pixel sensor and subsequently combine them to form a corresponding pixel signal.

*Corresponding author

 <kiran@tifr.res.in> (K.S. Gothe)

ORCID(s):

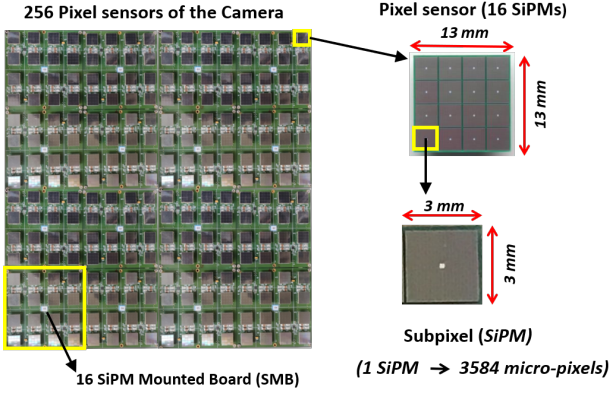


Figure 2: Camera pixel sensor matrix, a pixel sensor and a subpixel within a pixel sensor illustrated.

Table 1

Specifications of the SiPM pixel sensor, S13361-3050AS04 from Hamamatsu used in the camera (temperature=25°C; overvoltage= 3 V; Dark count measurement threshold=0.5 p.e.)

Parameter	Value
Size of the array of SiPMs	13 mm × 13 mm
Number of SiPMs in the array	16
Size of each SiPM	3 mm × 3 mm
Number of micro-pixels/SiPM	3584
Dark count rate	0.5 - 1.5 MHz
Crosstalk probability	3%
Gain	1.7×10^6
Breakdown voltage, V_{br}	53 ± 5 V
Recommended operating voltage, V_{op}	$V_{br} + 3$ V
Typical variation in V_{op} between the SiPMs in the array	0.1 V
Terminal capacitance of SiPM	320 pF

One of the goals of the IACT telescope is to detect gamma rays spanning energy range of few 100's of GeV to few 10's of TeV and accordingly, the front-end analog signal processing should support sufficiently large dynamic range in terms of number of photon equivalent (p.e.) counts. Equally important is the capability to measure single-p.e. gain for each pixel to estimate the number of incident photons. It also helps to tune the SiPM bias voltages for gain uniformity across all the pixels. A single-p.e. resolution demands a good Signal-to-Noise Ratio (SNR).

Section 2 describes the overall front-end of the camera which houses the preamplifiers. The preamplifier design goals and the constraints are presented in the section 3. Section 4 presents the actual design of the preamplifier to meet the requirements. The performance tests and their outcome are presented in the section 5. The concluding remarks are made in section 6.

2. Camera Front-end

The 256 pixel camera has front-end and back-end sections as shown in figure 3. The front-end electronics of the camera is divided into 16 identical modules called Pixel Cluster Module (PCM). A Sensors Mount Board (SMB) holds 16 pixel sensors with a pitch size of 22 mm. The light concentrators (LC) fixed in front of each pixel, guides the photons reflected by the light-collector of the telescope on to the pixel's active surface. The entry area of LC is ~ 21 mm × 21 mm and defines the angular resolution of $\sim 0.3^\circ$ for the camera. Four preamplifier circuit PCBs are directly plugged onto the SMB using four low pitch connectors to maintain signal integrity. The 16 subpixel signals from a pixel sensor are to be processed by each of the four channels in a preamplifier to form a corresponding pixel signal. A cluster digitizer module (CDM) in the back-end electronics receives 16 processed pixel signals from the preamplifiers in a PCM. These pixel signals are further amplified in CDM (see section 4) before trigger generation and the signal readout.

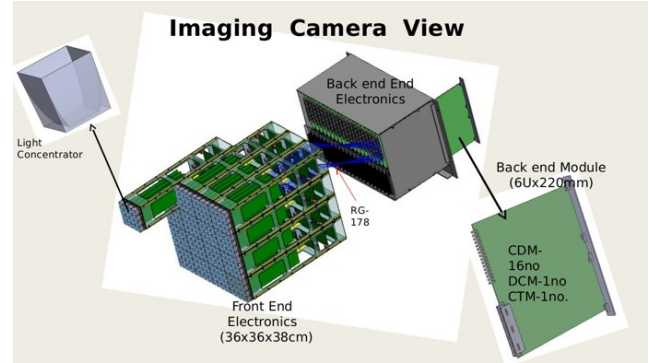


Figure 3: Schematic view of the camera structure showing front-end and back-end portion. The front-end comprises 4x4 array of pixel sensors and associated signal processing electronics.

3. Design goals and constraints

From physics consideration, the main goal for the preamplifier design is to have a wide dynamic range of 1-1500 p.e. per pixel. The wide dynamic range requirement stems from the requirement of wider energy spectrum of the detected gamma rays. Also, desired SNR in the single p.e. region under dark condition is more than 5.0 to have accurate pixel gain calibration. These goals are to be achieved following some design constraints as given below:

- As mentioned in section 2, the 4 channel preamplifier cards are directly plugged into the connectors mounted on the SMB and therefore the cards have to be mechanically aligned with the corresponding pixel sensors with the pitch size of 22 mm. The alignment requirement limits the maximum width of the 4 channel preamplifier PCB to less than 4 times the pitch size.

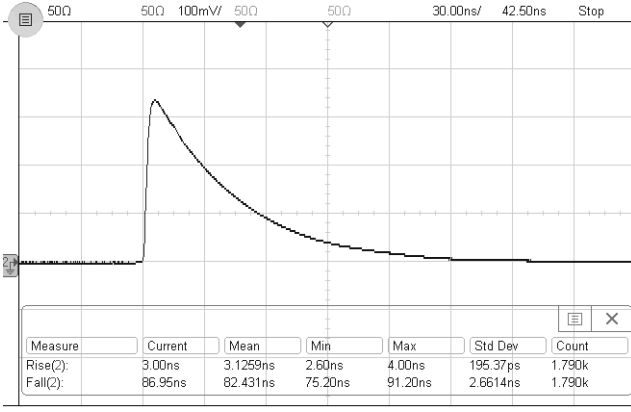


Figure 4: A raw pulse from a SiPM subpixel recorded on an oscilloscope with 500 MHz bandwidth. The SiPM biased at an overvoltage of 3 V was kept in a dark box. The anode of the subpixel was connected to the oscilloscope channel with 50 Ω termination. The pulse output from the anode was triggered by the nanosecond flashes of light incident on the SiPM.

- A pixel signal is to be formed by combining the 16 subpixel signals. This would lead to large component density, more power requirement and high electronic noise to deal with.
- Maximum power consumption for the front-end electronics to be kept below 0.5 W/pixel.
- A typical raw pulse from SiPM subpixel measured in a dark box test setup is shown in figure 4. The long decay time of the subpixel pulse (~ 80 ns) as seen in the figure is a result of large intrinsic time constant of the subpixel[6]. This poses a problem of larger noise integration.
- The bandwidth of the preamplifier should be high enough to accept fast rise time pulses from SiPM as seen in figure 4.
- pixel sensors are exposed to high night sky background (NSB) during the night observations. The pulses from SiPMs due to NSB would contaminate the pixel signal. Based on measurements carried out at Hanle, the estimated NSB would induce ~ 0.5 p.e. per subpixel over the duration of ~ 80 ns. The estimate assumes a photon detection efficiency (PDE) of 25% and LC efficiency of 65%. Under moonlit conditions, the NSB rate and therefore the rate of induced p.e.counts would go up by an order of magnitude.
- A large capacitance of the subpixel photosensor (see table 1) coupled with the input impedance of the front-end preamplifier may form a dominant time constant causing further elongation of tail of the subpixel pulse[6]. One way to bring down the components count of the circuit is to combine the subpixel signals before the preamplifier itself. But this would increase the sensor capacitance in multiples of ~ 320 pF. If the

Table 2

The technical requirement and the achieved results for the preamplifier.

Parameter	Required	Achieved
Size of the PCB	70 mm \times 110 mm	70 mm \times 110 mm
Input impedance	$<25 \Omega$	$\sim 6 \Omega$
Signal pulse width (FWHM)	<12 ns	11 ns
Rail Voltages	± 3.3 V	± 3.3 V
Single p.e. amplitude with 50 Ω load; over-voltage, $V_{ov}=3$ V	<0.7 mV	0.7 mV
SNR under dark condition @single p.e. @ $V_{ov}=3$ V	>5.0	5.8
Dynamic range	1-1500 p.e.	1-1600 p.e.
Power	<0.5 W per pixel	~ 0.5 W per pixel
Cost per pixel	<5000 INR	4500 INR

input impedance of the preamplifier is not sufficiently low, the increased capacitance would result in longer decay time beyond its nominal value of ~ 80 ns.

The important implication of these constraints is that it has to be a low power, low noise and wide bandwidth circuit with low input impedance and that has just few millimeters of PCB width available for each subpixel signal processing circuit. The analog signal processing circuit design is discussed in detail in the next section.

4. Analog Processing Chain

Based on the physics goals and the various constraints described in section 3, the technical requirements for the design of the preamplifier are given in the table 2.

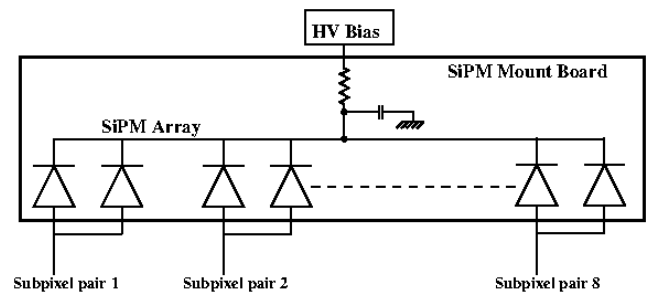


Figure 5: subpixel summing before preamplifier. 2 adjacent subpixels outputs are shorted to form 8 subpixel pair signals.

In order to meet these requirements, the preamplifier circuit topology is chosen to have following main features:

- Every adjacent subpixel pair is combined to form a subpixel pair signal just by shorting their anodes (figure 5) before the input of the preamplifier itself. The combined capacitance of the subpixel pair would be 640 pF and this calls for an extremely low input impedance of the preamplifier.
- All the eight subpixel pair signals from a pixel are separately processed before they are summed using summing amplifier stage.
- To facilitate the single-p.e. gain calibration more accurately, enable-disable feature is incorporated in the design for every subpixel pair.
- The long tail of the subpixel pair signals are shortened by pulse shaping before summing them in order to reduce the chance of noise pulses primarily due to NSB overlapping signal.

The topology consists of 4 different stages in cascade as shown in figure 6. The circuit takes 8 subpixel pairs' signals

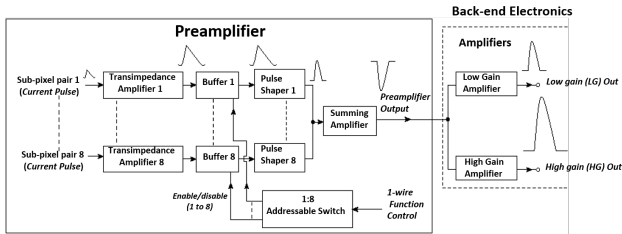


Figure 6: Topology of the preamplifier chain for a pixel consisting of 16 subpixels grouped into 8 subpixel pairs

as inputs. The signals are converted into voltage pulses using a transimpedance amplifier (TIA). The TIA outputs are buffered for impedance matching with pulse shaping circuit. Pulse shaping is achieved using pole-zero cancellation technique. The shaped subpixel pulses are then added using a summing amplifier to form a pixel output.

Two designs ideas were considered for TIA stage; first one using high bandwidth operational amplifier[4] and the other using RF NPN transistor (BFR182) in common base configuration[3]. From the power requirement consideration, the later choice was considered. In common base amplifier configuration, input capacitance does not suffer from miller effect and hence the bandwidth is not compromised. Since the collector capacitance is very small, the collector resistance and hence the transimpedance can be relatively large without compromising speed. The high transimpedance also imply less stringent noise demand in the subsequent signal processing stages. The quiescent emitter current of of the transistor is set at ~ 4 mA which ensures a very low input impedance of around $\sim 6 \Omega$. The quiescent power drawn from the dual supply voltage of ± 3.3 V is ~ 26 mW which is much lower when compared to the TIA design based on some high bandwidth operational amplifiers such as OPA846.

The buffer stage is introduced to match the impedance of the TIA output to that of the pulse shaping circuit. Based

on the factors like power, noise and bandwidth the op-amps OPA846 and OPA691 from Texas Instrument were given consideration for the buffer circuit and also for summing amplifier circuit. OPA846 offers better performance noise wise ($1.2 \text{ nV}/\sqrt{\text{Hz}}$, $2.8 \text{ pA}/\sqrt{\text{Hz}}$) compared with OPA691 ($1.7 \text{ nV}/\sqrt{\text{Hz}}$, $15 \text{ pA}/\sqrt{\text{Hz}}$). However, OPA691 was chosen due to its lower supply current of 5.1 mA as compared to 13.2 mA specified for OPA846. Another important reason for choosing OPA691 is that it offers a provision to disable the output putting it in high impedance state. This provision is used to achieve more accurate in-situ calibration of the preamplifier gain. The disabling 7 out of 8 subpixel pair processing chain puts the corresponding outputs of the buffers in high impedance state, thus eliminating noise contribution from the disabled processing chain. This improves the SNR at single-p.e. level and therefore accuracy in gain estimation. The pulse shaping circuit shortens the tail portion of the signal. It is based on the pole-zero cancellation technique which is realized using passive components.

The fourth and the last stage of the preamplifier circuit is an inverting summing amplifier using OPA691 that adds the 8 subpixel pairs' signals coming from shaping circuits. The amplifier gain is tuned so that full output swing of OPA691 is utilized to cover the required dynamic range.

A pixel signal from the preamplifier is further amplified in the back-end electronics as shown in figure 6 using dual gain stages in parallel leading to low gain (LG) and high gain (HG) outputs of the pixel. LG and HG outputs for each pixel are digitized as separate channels[7]. This feature helps to achieve the required dynamic range without going for expensive high resolution ADC.

5. Performance

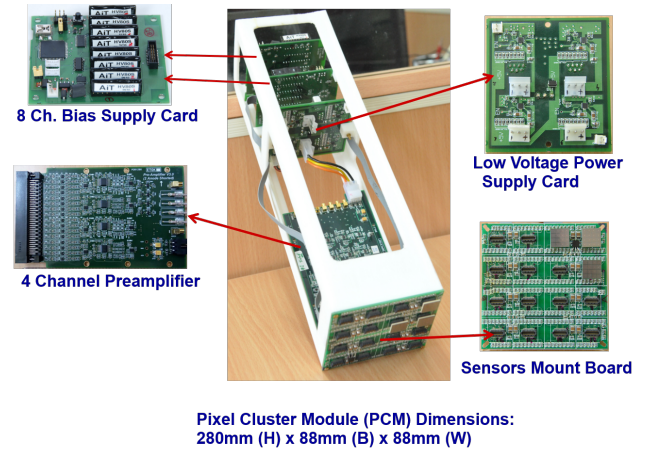


Figure 7: PCM and its constituent circuit boards.

Table 2 summarises the important design objectives and the corresponding performance results. Figure 7 shows an assembled PCM with its constituent PCBs viz. SMB that holds 16 pixel sensors, four preamplifier cards which get plugged into the 80-pin low pitch connectors on the

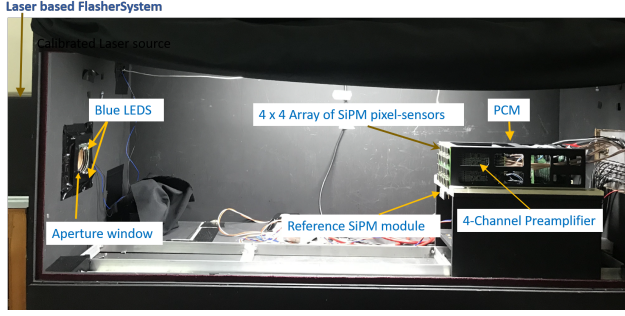


Figure 8: Dark box test setup for evaluating performance of the front-end electronics of the Camera. Pulsed light from the flasher system enters the dark box through the circular window seen on the left. The blue LEDs near the window can be used to simulate NSB.

SMB, two SiPM bias cards and a low voltage power supply providing power to preamplifiers (± 3.3 V) and bias cards (+5 V).

A light-tight dark box test setup for evaluating PCM performance is shown in figure 8. pixel sensors mounted on the SMB of a PCM are exposed to the periodic sub-nanosecond pulses of diffused light from a flasher system. The flasher system is based on a 355 nm sub-nanosecond pulsed laser STV-01E-140 from Teem Photonics and employs a set of neutral density (ND) filters to set the required intensity of the light and integrating sphere to diffuse the light before sending it out. The gain of the each SiPM pixel sensor can be adjusted by varying the biasing voltage supplied by bias cards in the PCM. The pixel signals from the preamplifier triggered by the light flashes are further amplified using LG and HG stages in CDM. The LG and HG outputs for each pixel are then digitized and recorded using a commercial digitizer module, V1742[8] at a sampling rate of 1GSPS. Eventually, the camera integrated tests were performed successfully, wherein the preamplifier output signals were amplified, digitized and recorded solely using the back-end modules in the camera like CDMs, CTM and DCM[7].

5.1. Gain uniformity across subpixel pairs

Dispersion in the gains of the signal processing of 8 sub-pixel pairs prior to summing contributes to the uncertainty in the estimate of detected number of photons, thereby affecting the detection resolution. In order to estimate the error in gain uniformity, dark box test setup was used. At a particular pulsed light intensity, the preamplifier outputs were recorded while the number of subpixel pairs contributing to the pixel signal were increased one by one starting from 0 to 8. Here, the programmable subpixel pair enable/disable feature of the design was made use of to add or remove subpixel pair contribution. A representative plot of the measured amplitudes of the preamplifier output against the number of contributing subpixels is shown in Figure 9. The linearity error is below 3% as seen in the error plot in the same figure.

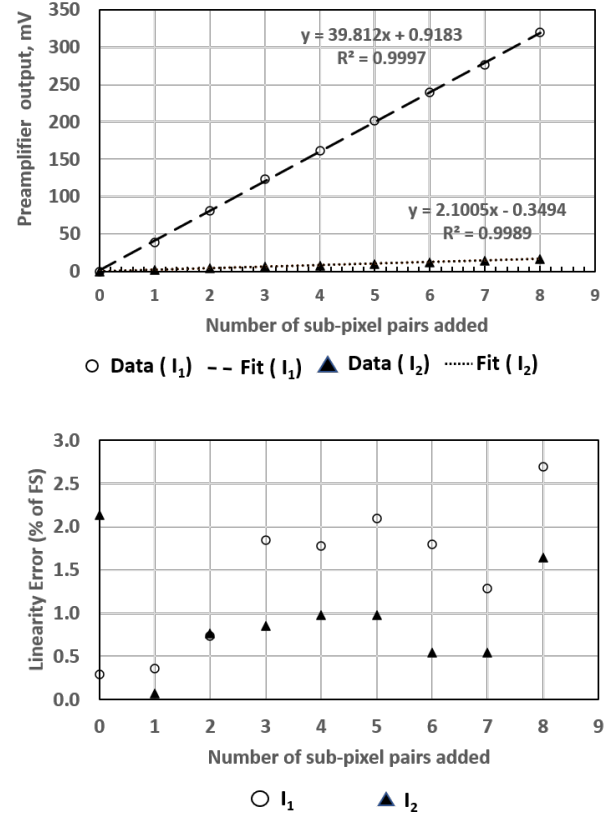


Figure 9: Pixel output from preamplifier as a function of the number of subpixel pairs enabled (top) for two arbitrarily selected pulsed light intensities, I_1 & I_2 . The plot at the bottom shows the corresponding errors in linearity in terms of per cent of full scale reading.

5.2. Pulse shaping

Figure 10 shows a pixel output from the preamplifier in response to a light pulse from the flasher system falling on the SiPM pixel sensor. The rise time of the trailing edge of the pulse is reduced to ~ 8 ns thereby limiting the FWHM to ~ 11 ns. The advantage of signal pulse shaping in the

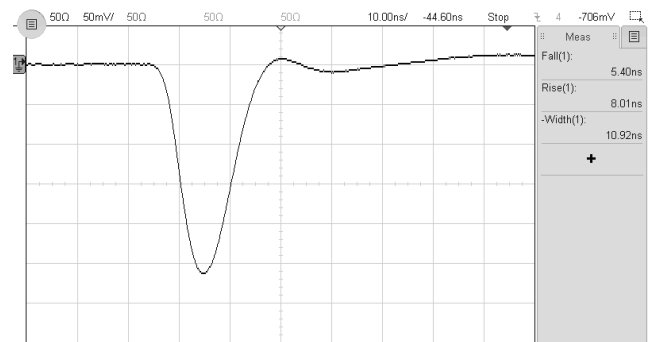


Figure 10: A typical response of a preamplifier in the dark box setup to the pixel sensor signal triggered by the light pulses from the flasher system.

presence of background light mimicking NSB was evaluated

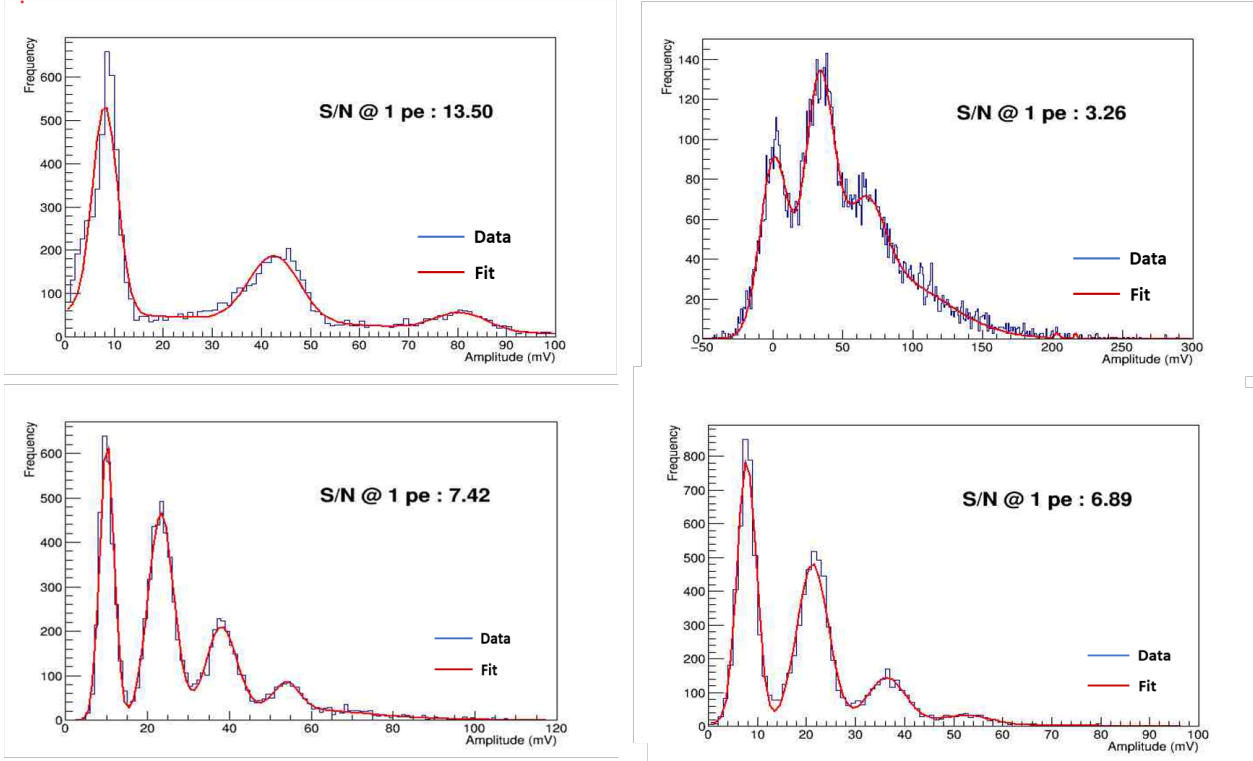


Figure 11: Amplitude distribution for one of the pixels obtained for 4 different combinations of the settings. Top left: no pulse shaping & LEDs turned off; top right: no pulse shaping & LEDs turned on; bottom left: pulse shaping & LEDs turned off; bottom right: pulse shaping & LEDs turned on.

quantitatively using a dark box test set-up (Figure 8). The data was recorded for a channel under four different combinations of the settings as mentioned below:

- no pulse shaping; simulated NSB turned off
- no pulse shaping; simulated NSB turned on
- with pulse shaping; simulated NSB turned off
- with pulse shaping; simulated NSB turned on.

To simulate NSB in the dark box, the intensity of the light from the LEDs was adjusted to make background light match the estimated NSB at Hanle. The estimate of the photon rate due to simulated NSB was obtained from the observed baseline shift in the SiPM response[9]. The data recording was triggered by light pulses of low intensity. Figure 11 show the pulse height spectra corresponding to a preamplifier output for a pixel under 4 different combinations of the settings mentioned above. The intensity of laser light is kept sufficiently low so as to give average pulse height in the single-p.e. region. Therefore, in each of the spectrums, the first peak is pedestal and the subsequent peaks correspond to 1 p.e., 2 p.e. and so on. While calculating SNR, the difference between the 1-p.e. peak and pedestal peak is taken as signal whereas the standard deviation of the pedestal peak is taken as noise.

It is seen from the figure 11 that there is a deterioration of SNR when the NSB is introduced which is as expected.

However, comparison of the spectrums obtained with and without pulse shaping shows that despite reduction in the signal strength, the achieved SNR is better with pulse shaping.

5.3. Crosstalk measurement

The channel-to-channel crosstalk in 4 channel preamplifier cards were measured by injecting current pulses to all the subpixel pair inputs of a channel and recording the voltage pulses at all the channel outputs of the preamplifier. Here, the voltage pulse from pulse generator (Agilent, model:81150A) was converted to a current pulse using a series resistor of 1 k Ω that is quite large compared to the preamplifier input impedance of 6 Ω . Figure 12 shows typical crosstalk measured for one of the preamplifier cards. The values shown are in percentage with respect to output of the injected channel. The measurements carried out for each preamplifier card in the camera have shown the crosstalk to be less than 1%.

5.4. Single photo-electron resolution

Pulse profiles for all the pixel signals at the output of HG amplification stage were recorded using the dark box setup described earlier. The data recording was triggered using low intensity laser pulses bombarded on the pixel sensors to ensure operation in the single-p.e. region. Also, only one subpixel pair was enabled prior to the data recording, thus, eliminating the noise contribution from signal processing electronics of remaining seven subpixel pairs. Amplitude

Crosstalk in % with respect to pulse injected channel output voltage				
Preamplifier output channel number	1	2	3	4
4	0.5	0.5	0.5	
3	0.5	0.5		0.3
2	0.4		0.5	0.3
1		0.8	0.8	0.7
	1	2	3	4
Pulse injected channel number				

Figure 12: A representative matrix of crosstalk measurements for a 4 channel preamplifier card.

spectrum of a representative pixel output in the region of single-p.e. is shown in figure 13. The distinct peaks from left to right in the figure correspond to pedestal, 1-p.e., 2-p.e. etc. The SNR is determined from these well separated pedestal and signal peaks as mentioned in section 5.2. The SNR value at 1-p.e. averaged over all the pixels is 6.0 for the SiPM overvoltage of 3 V, which is well above the targeted value of 5.0.

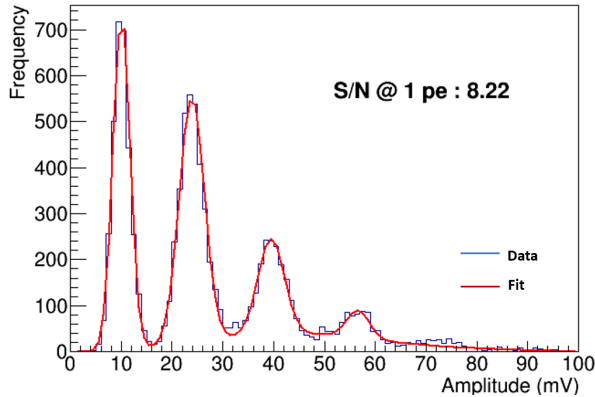


Figure 13: The distribution of amplitudes of pulses at the HG channel output for a representative pixel wherein only single subpixel pair was enabled. Leftmost peak is the pedestal peak followed on the right by signal peaks. The SiPM pixel sensor was biased at 3 V overvoltage. The data was triggered by the low intensity light pulses from the flasher.

5.5. Linear dynamic range

The intensity of the light pulses from the flasher system in the dark box setup is controlled by using different combinations of neutral density (ND) filters. The variation in the density of photons of a light pulse in the plane of pixel sensors was measured in a separate exercise. The photon density was found to vary by less than $\sim 3\%$ over a distance of 20 cm in the region centered around the pixel sensors. A reference SiPM (Hamamatsu, S12572-050C) mounted on a SiPM evaluation kit (Hamamatsu, C12332-01)[10] was also placed next to the pixel sensors as shown in the figure 8. The pixel sensors of the PCM and the reference SiPM are

positioned within a distance far less than 20 cm ensuring that the intensity of pulsed light seen by the reference SiPM does not differ from that of the pixel sensors by more than 3%.

In another important exercise, output pulses from the reference SiPM triggered by the pulsed light under different filter combinations were recorded. The recorded data were used to calibrate the ND values of the filter combinations in terms of number of photons detected by the pixel sensors.

Finally, to evaluate the linear dynamic range of the preamplifier, the pulse profiles from the LG channel outputs were recorded for different filter settings. Figure 14 shows a linear dynamic range of LG output up to 1600 p.e. for a representative pixel. Here, the number of detected photons on x-axis are derived from the ND values of the filter setting based on the calibration exercise mentioned above. As seen in the figure, the typical estimate of the linearity error is less than 3.5% which is well within our design target.

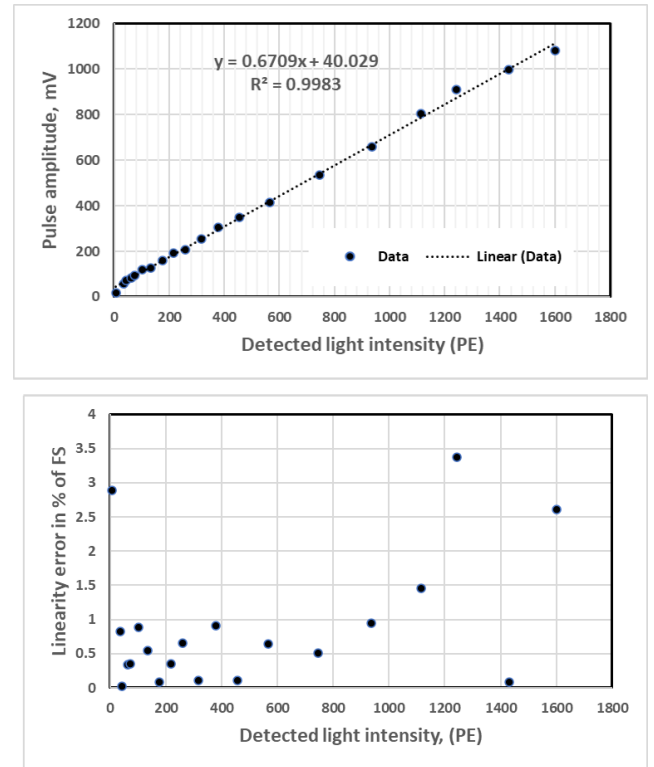


Figure 14: Linear dynamic range of photon detection. Left plot shows the amplitude of the LG output pulse with the light intensity detected by the pixel sensor and corresponding linearity errors are shown in the right plot. The SiPM pixel sensor was biased at 3 V overvoltage. The data was triggered by the pulsed light from flasher system with different filter settings.

6. Conclusion

We have successfully designed and tested the preamplifier circuit that processes analog signals from large size off-the-shelf pixel sensor available in the form of 4×4 array

of SiPMs. In spite of the application specific severe design constraints, the preamplifier has met all the requirements successfully as demonstrated in the laboratory tests. To meet these requirements, the circuit has implemented a judicious combination of some design strategies and circuit ideas. Table 2 summarises the desired and achieved specifications of the preamplifier. The performance tests carried out in the dark box setup confirmed the linear dynamic range from 1 to 1600 p.e. signal detection. We also achieved the average SNR of ~ 6.0 , at single-p.e. level under dark condition for 3 V overvoltage which is more than the specified design goal of 5.0.

Acknowledgements

We acknowledge the support of the Department of Atomic Energy, Government of India, under project identification number RTI 4002. We thank our group members Mr Santosh Chavan, Mr A P Krishnan Kutty, Mr Piyush Verma and Ms Varsha Nikam for their support to this project.

Declaration of competing interest

The authors declare that they have no known competing financial interests or personal relationships that could have appeared to influence the work reported in this paper.

References

- [1] R. Koul et al., The TACTIC atmospheric Cherenkov imaging telescope, Nucl. Instrum. Methods Phys. Res. A, Volume 578, Issue 3, 11 (2007), 548-564
- [2] N. Bhatt, et al., Status update of the MACE Gamma-ray telescope, Proceedings of Science, ICRC2021, 756, 2021
- [3] H. Anderhub, et al., Design and operations of fact – the first G-APD Cherenkov Telescope, J. Instrum. 8(2013).
- [4] J A Aguilar, et al., The front-end electronics and slow control of large area SiPM for the SST-1M camera developed for the CTA experiment, Nucl. Instrum. Methods Phys. Res. A 830 (2016) 219-232
- [5] Hamamatsu Photonics, MPPC Arrays 13361-3050 series Datasheet, https://www.hamamatsu.com/content/dam/hamamatsu-photonics/sites/documents/99_SALES_LIBRARY/ssd/s13361-3050_series_kapd1054e.pdf, (Accessed on 2022-08-16)
- [6] F. Corsi et al., "Electrical Characterization of Silicon Photo-Multiplier Detectors for Optimal Front-End Design," 2006 IEEE Nuclear Science Symposium Conference Record, 2006, pp. 1276-1280, doi: 10.1109/NSSMIC.2006.356076.
- [7] Sandeep Kumar et al., Development of a Prototype 16-channel Dual Gain Waveform Readout and Data Transfer System for IACT based Telescope Camera, Nucl. Instrum. Methods Phys. Res. A (2022), Submitted for publication
- [8] CAEN, V1742 Technical specifications, <https://www.caen.it/products/v1742/> (Accessed on 2022-08-16)
- [9] A. Nagai et al., SiPM behaviour under continuous light, 2019 JINST 14 P12016
- [10] https://www.hamamatsu.com/content/dam/hamamatsu-photonics/sites/documents/99_SALES_LIBRARY/ssd/c12332-01_kacc1233e.pdf (Accessed on 2022-08-16)